Scientific Research Publishing

Optics and Photonics Journal, 2022, 12, 201-213
https://www.scirp.org/journal/opj
ISSN Online: 2160-889X
ISSN Print: 2160-8881

Fabrication of Polarization Control Devices Using Metal Grating Structures

Atsushi Motogaito, Yukino Hayashi, Akinori Watanabe, Kazumasa Hiramatsu

Graduate School of Engineering, Mie University, Tsu, Japan
Email: motogaito@elec.mie-u.ac.jp

How to cite this paper: Motogaito, A., Hayashi, Y., Watanabe, A. and Hiramatsu, K. (2022) Fabrication of Polarization Control Devices Using Metal Grating Structures. *Optics and Photonics Journal*, **12**, 201-213.
https://doi.org/10.4236/opj.2022.129015

Received: September 9, 2022
Accepted: October 28, 2022
Published: October 31, 2022

Abstract

A polarization control device was developed using a plasmonic metasurface with the aim of achieving the desired polarization state. In this study, the Ag metal grating structure was fabricated as a plasmonic metasurface by electron beam lithography and a lift-off process. The phase difference of the fabricated sample was 21.0˚. This value is almost consistent with the simulation (24.0˚). Then, the transmission and phase difference is dependent on the structural parameter. Because of the propagation of surface plasmon polariton at the interface between Ag and SiO_2 or Ag and air, it is believed that the transmittance and the phase difference for TM polarized light can be controlled by the structural parameters. By plotting on the Poincaré sphere after calculating the S-parameter by simulation, it is clear that the arbitrary polarization status can be controlled by the structural parameter.

Keywords

Surface Plasmon, Metal Grating, Polarization Control, Plasmonic Metasurface

1. Introduction

Polarization devices, such as a polarizer, beam splitter, wave plate, and optical retarder, are often used for controlling the polarization state and realizing the specific polarization light. For these devices, solid birefringence materials, such as crystal, mica, CaF_2, and MgF_2 or polymer materials, such as polyvinyl alcohol, are often used. Although solid birefringence materials are stable against temperature changes, they are difficult to process and reduce in size and thickness. However, since polymer materials are used in the form of thin films, they can easily be made smaller and thinner, but they are more sensitive to temperature changes and have low fracture thresholds. To solve these problems, plasmonic metasurfaces such as wire grid structures have been proposed. The basic polari-

zation device using plasmonic metasurfaces is the wire grid polarizer. In 1893, Hertz used a wire grid structure as a polarizer for the first time [1]. Then, the wire grid polarizer for infrared light was fabricated in the 1960s [2] [3] [4]. The development of the fabrication method of nanostructures, such as electron beam lithography, nanoimprint lithography, subwavelength lattice, or nanowire, was used to realize the wire grid polarizer for the near infrared, visible, and ultraviolet regions [5]-[14].

Recently, wire grid polarizers using surface plasmon resonance or chiral metamaterial have been realized [15] [16] [17] [18]. Furthermore, the waveplates or optical retarders can be realized by surface plasmon resonance [19] [20] [21] [22]. The proposed device with metal nanostructures changes the transmittance and phase difference by means of a surface plasmon resonance, which is controlled by the periodic nanostructure. The advantages of such a device are that it is easy to make it smaller and thinner, it is stable against temperature changes, and it is possible to obtain various polarization states for each structure. The key disadvantage is that the transmittance is inferior to that of both solid crystals and polymer films due to the use of metal. However, we describe here an extraordinary transmission phenomenon that occurs due to surface plasmon resonance in metal diffraction gratings [23]-[34]. It is believed that by exploiting this phenomenon, the transmittance can be improved. We have previously reported the surface plasmon sensor [25] [26] and the perfect absorber with the selectivity of wavelength [27].

We aim to realize polarization controlling devices with plasmonic metasurfaces such as one-dimensional metal grating structures. The merit of using a plasmonic metasurface is that the transmittance and phase of light can be controlled using structural parameters such as the period, duty ratio, and metal thickness. If the transmittance and phase of light can be controlled using structural parameters, the elliptical polarization can be controlled arbitrarily. Some reports describe the process of controlling the state of polarization. N. Vanstleenkiste *et al.* reported the use of remote control to create polarization Configurations for the purpose of laser cooling atoms [28]. A. Jullien *et al.* reported the controlling polarization status of nonlinear materials [29]. C. Gao *et al.* reported the use of a multilayer dielectric grating structure to create a polarization-controlled grating polarizer [30]. P. C. Wu *et al.* reported a broadband wide-angle multifunctional polarization converter in the electromagnetic wave region using a liquid-metal-based metasurface [31]. J. P. Balthasar Mueller presented two independent and arbitrary phase control devices in the visible region utilizing a TiO_2 metasurface [32]. A. Arbabi *et al.* reported on the control of phase and polarization by dielectric metasurface [33]. P. Lovera *et al.* reported polarization tunable transmission in the visible and near infrared regions via plasmonic arrays [34]. Recently, T. Yan, *et al.* reported the circular polarization hologram realized by Pancharatnam-Berry phase in microwave frequency [35]. The polarization device described above is capable of converting a specific polarization state, e.g., linearly polarized or circularly polarized light, into another polarized state.

There are some kinds of applications, such as polarimeters [36] [37], optical coherence tomography [38] [39], laser micro-machining [40], and color filters [41]. In particular, our new polarization-controlled devices are effective for application to polarization sensitive optical coherence tomography (PS-OCT). This technique uses polarized light to observe additional structural details in samples, particularly biological samples that cannot be observed otherwise. J. S. Amaya *et al.* reported the web control system for transcorneal electric stimulation devices for observing biological samples [42]. Using our new polarization-controlled device, it is expected that the performance of PS-OCT will be improved using light in a specific polarized state in which the polarized state is controlled. In particular, PS-OCT is used to investigate diseases inside the eye in fundus examination. PS-OCT often uses linearly polarized light, but in order to obtain a clearer image considering birefringence and depolarization effects in the retina, it is necessary to develop an optical element that can obtain any elliptically polarized light.

In this study, in order to realize arbitrary elliptical polarization, a polarization control device using a one-dimensional metal grating as a plasmonic metasurface is realized with the aim of obtaining such a desired elliptical polarization state.

2. Simulation and Experimental Methods

2.1. Simulation Method

The polarization control device was designed by the rigorous coupled-wave analysis (RCWA) method in which structure-dependent polarization characteristics of the device were simulated. The input parameters, variables calculated by the RCWA method, and output variables described here are summarized in **Table 1**.

The polarization control device consisted of a metal grating structure fabricated on SiO_2 substrate as shown in **Figure 1**. The simulation variables were the wavelength of the incident light (λ) and the structural parameters of the grating pitch (P), the metal thickness (t), and the duty ratio (D), which is the ratio of the width of the metal structures to the pitch. In this study, the wavelength used was 532 nm and the metal was Ag. Using the RCWA method, the amplitude transmittance of TE and TM light (t_{TE} and t_{TM}) and the phase difference with respect to incident light for TE and TM light (Δ_{TE} and Δ_{TM}) were calculated. From these values, the effective transmission (t_{rms}), the retardation (Δ), and the ratio of the amplitude transmittance (ψ) can be obtained. The flowchart of this calculation is shown in **Figure 2**.

2.2. Experimental Method

Then, the designed device was fabricated by electron beam lithography, sputtering, and lift-off. The phase difference realized with the manufactured device was measured using the Senarmont method.

Table 1. The input parameters, variables calculated by the RCWA method, and output variables. (a) Input parameter; (b) Calculate variables; (c) Output variables.

(a)	
Incident wavelength	$\lambda = 532$ nm
Structural period	P
Width of Ag stripe	w
Thickness of Ag	t
Duty ratio	$D = w/p$
(b)	
Phase (TM)	Δ_{TM}
Amplitude transmittance (TM)	t_{TM}
Phase (TE)	Δ_{TE}
Amplitude transmittance (TE)	t_{TE}
(c)	
Phase difference	$\Delta = \Delta_{TM} - \Delta_{TE}$
Effective transmittance	$t_{rms} = \mathrm{sqrt}\left(t_{TM}^2 + t_{TE}^2\right)$
Ratio of transmittance	$\tan\Psi = t_{TE}/t_{TM}$

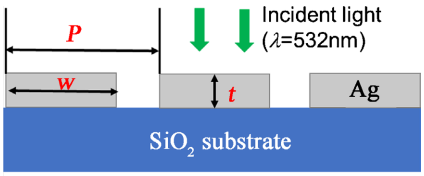

$$\text{Duty ratio(D)} = \frac{Width\ of\ Ag\ stripe\ (w)}{Structual\ period\ (P)}$$

Figure 1. Schematic of the polarization control device consisted of a metal grating structure fabricated on SiO_2 substrate. The grating period (P), thickness of Ag (t), width of Ag (w), and duty ratio D (w/P) are the parameters of the designed structure. The wavelength of the incident light (λ) is 532 nm.

The substrates used were made of 1-mm-thick quartz glass. Prior to spin-coating the electron beam (EB) resist, hexamethyldisilazane (HDMS) was spin-coated on the surface of the quartz glass substrate to improve the adherence between the substrate and the EB resist. The surface was spin-coated with an EB-positive resist (ZEON, ZEP-520A), after which prebaking was performed. Subsequently, a charge-up prevention treatment was spin-coated on the EB resist. The electron beam lithography (EBL) system (Crestec CABL-8000) was equipped with a ZrO/W thermal field-emission cathode. The acceleration voltage was 30 kV; electrons accelerated at this voltage were able to penetrate the resist. After exposure, the resist was developed, resulting in the binary diffractive lens. The size of the pattern for the sample was 1.5 × 1.5 mm^2. Then, Ag was sputtered on the sample by

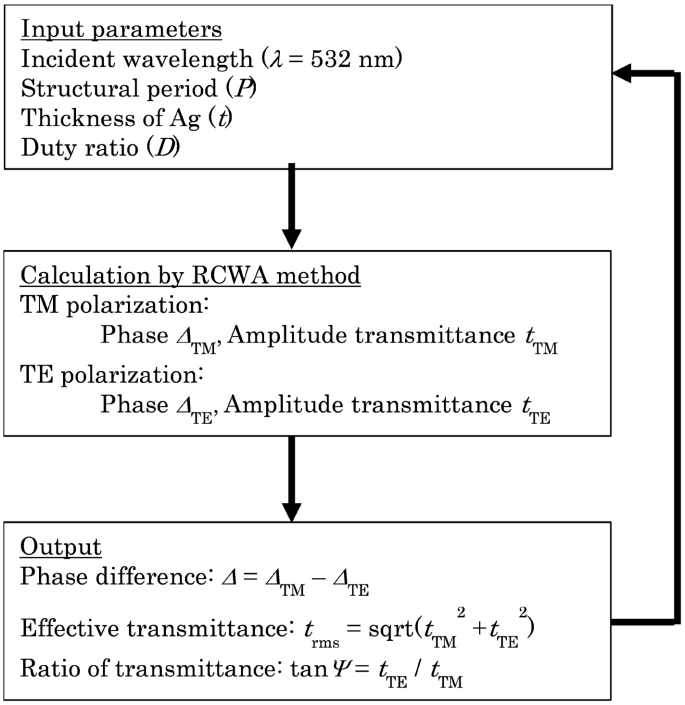

Figure 2. Flowchart of the calculation of the polarization characteristics of the designed device. The λ, P, t, and D are input parameters. By rigorous coupled-wave analysis method, phase difference, effective transmittance, and ratio of the transmittance are obtained.

using DC magnetron sputtering equipment (SANYU, SC-701Mk II ADVANCE) and the target structure was obtained after lift-off. The fabricated sample was observed by scanning electron microscope (SEM).

Thereafter, the phase difference of the fabricated sample was characterized using the Senarmont method. First, the laser light is squeezed from a light source with a 2-μm pinhole and a polarizer is used to create linearly polarized light that oscillates in the horizontal (x-axis) direction. When this is incident on an unknown sample with a phase difference δ placed in a direction in which the slow axis forms a 45˚ angle, elliptically polarized light whose axis is tilted by θ is generated. After that, the elliptically polarized light is returned to the linearly polarized light tilted by θ by injecting light onto the 1/4 wave plate whose slow-phase axes coincide vertically. The measurement is performed by rotating the analyzer with this angle θ placed in the y-axis direction. The final phase difference δ, is obtained by $\delta = 2\theta$.

3. Results and Discussion

3.1. Results of Simulation and Experiments

Figure 3 shows the surface SEM image of the sample after the lift-off process. The thick and dark part is the thin line part of Ag, and the thin and bright part is the surface of the glass substrate. This sample was designed as P = 360 nm, D = 0.7, and t = 30 nm. From this photograph, it was possible to prepare a sample

almost as designed.

Then, the phase difference between TE and TM light is characterized by simulation and experiment. The simulation of the phase difference with respect to incident light for TE and TM light (ΔTE and ΔTM) is shown in Figure 4. In these figures, the incident light is propagating in the $+z$ direction. This is the surface of the sample at $z = 0$. The transmitted light and the reflected light appear at $z = 0$. The phase difference of the transmitted light with respect to incident light is obtained as $\Delta_{TM} = +2.2^\circ$ (phase lag) and $\Delta_{TE} = -21.4^\circ$ (phase lead). The phase difference between TM and TE light is obtained as $\Delta = \Delta_{TM} - \Delta_{TE} = 24.0^\circ$.

However, the experimental result can be obtained by the Senarmont method. The result of the Senarmont method is shown in Figure 5. From this result, the

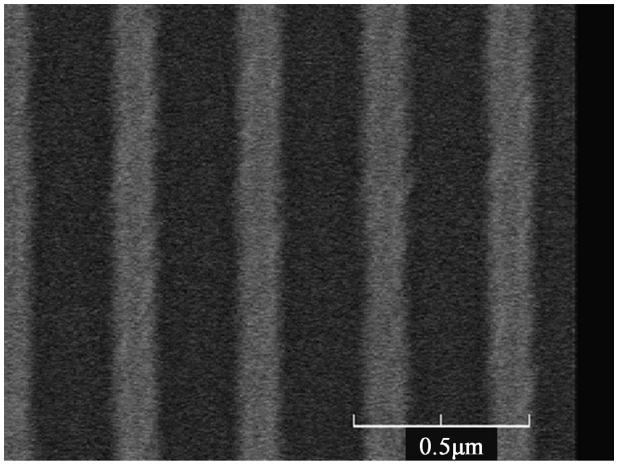

Figure 3. Surface scanning electron microscope image of the sample after the lift-off process. The dark part is Ag (w = 360 nm), and the bright part is SiO_2.

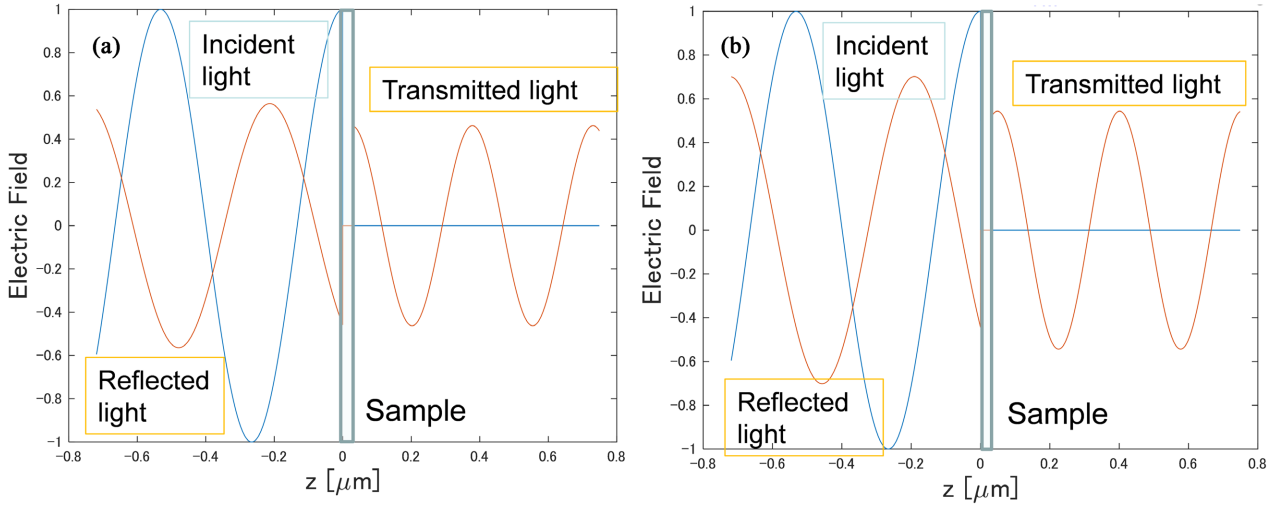

Figure 4. Simulation results of the phase difference with respect to incident light for Transverse Magnetic (TM) (a) and Transverse Electric (TE) light (b) (Δ_{TM} and Δ_{TE}). Light enters vertically from the left side of the sample and passes through the right side of the sample. Δ_{TM} is +2.2˚ (phase lag) and Δ_{TE} is −21.2˚ (phase lead). The phase difference between TM and TE light is +24.0˚ ($\Delta = \Delta_{TM} - \Delta_{TE}$).

phase difference can be obtained as $\Delta = 2\theta = 21.0^\circ$. Therefore, it is believed that the results of the simulation and the experiment are almost identical.

3.2. Discussion

Then, the dependence of the 0th transmittance and phase difference on the structural period is calculated as shown in Figure 6. From Figure 6(a), TE transmission is almost constant throughout the structural period, whereas TM transmittance depends on the structural period. The transmittance peaks can be obtained at 364 and 532 nm which are indicated by black and red arrows, respectively. Additionally, the abrupt phase difference changes from negative to positive and the phase lag for TM light can be obtained at 364 nm and 532 nm, whereas the phase difference for TE light is almost constant, as shown in Figure 6(b). Thus,

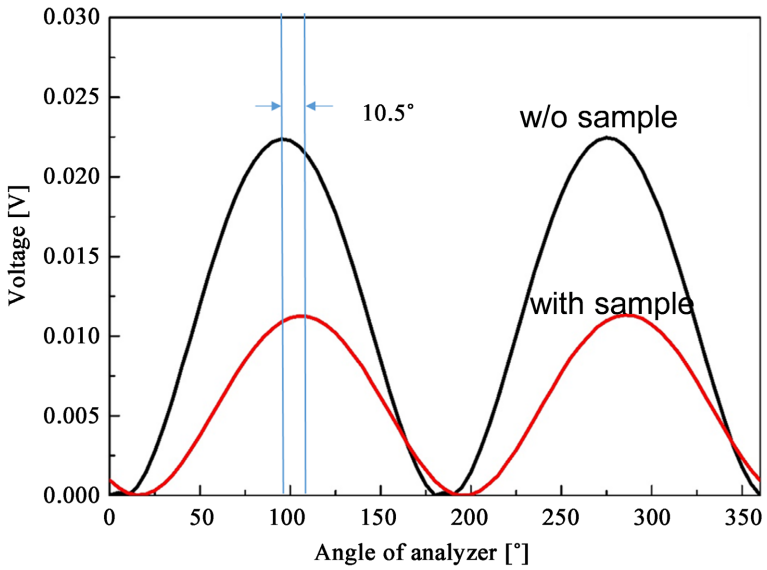

Figure 5. Experimental result obtained via the Senarmont method. Voltage indicates the intensity of the photodiode's output. From this experiment, the phase difference obtained is 21.0˚.

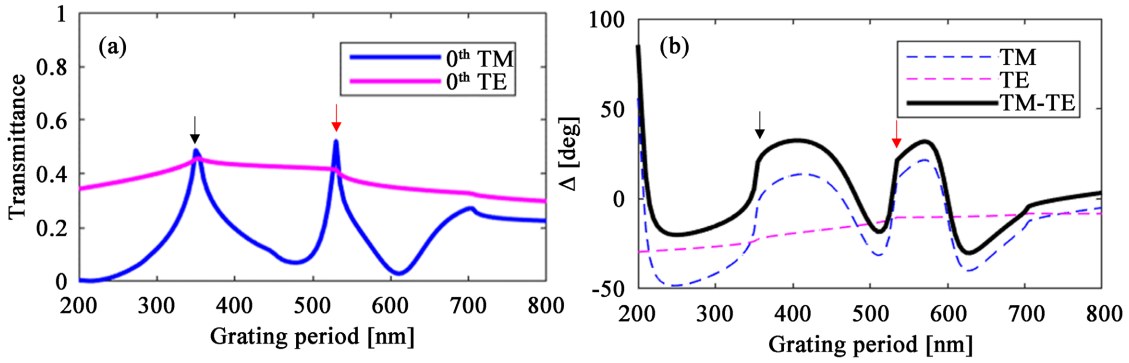

Figure 6. (a) Calculation of the dependence of the transmittance and (b) phase difference on structural period. The peak transmittance and the abrupt change of phase difference (from minus to plus) can be obtained at P = 364 nm and 532 nm). The black and red arrows indicate the period obtained the peak transmittance and the abrupt change of phase difference.

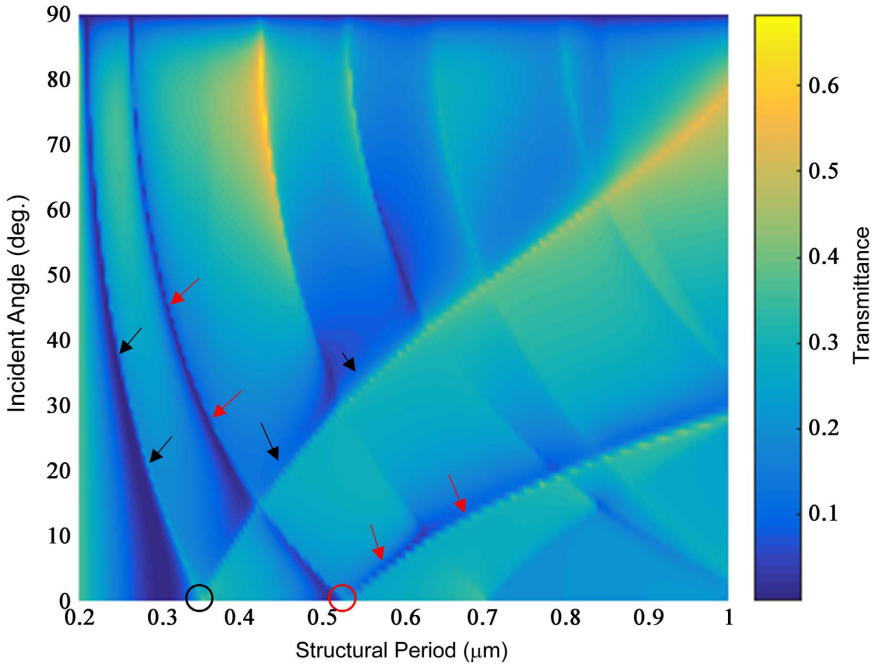

Figure 7. Transmittance mapping for TM light. The horizontal and vertical lines show the structural period and incident angle, respectively. The color bar indicates the transmittance. Some loci are found in the mapping. These loci indicated by black and red arrows refer to the condition of the exciting surface plasmon polariton at the interface between air and Ag or SiO_2 and Ag. They are obtained by the excitation condition of the propagating surface plasmon polariton.

the phase difference (Δ) is proportional to the phase difference of TM light.

The peak TM transmittance and the abrupt change in phase difference between 364 and 532 nm are attributed to the excitation of the propagating surface plasmon polariton in the one-dimensional (1D) Ag grating structure. The transmittance mapping for TM light is shown in **Figure 7**. The horizontal line shows the structural period, while the vertical line shows the incident angle. The color bar means the transmittance. There are some loci of the peak transmittance in **Figure 7**. In particular, the most important loci related results of **Figure 6** are indicated using black and red arrows. The circles at 364 and 532 nm indicate the peak transmittance at normal incidence related to **Figure 6**. According to our past study, these loci refer to the condition of the exciting surface plasmon polariton at the interface between air and Ag or SiO_2 and Ag [23] [24]. To determine the interface at which these loci are propagating surface plasmon polaritons, the intensity distribution of the magnetic field at 364 and 532 nm is calculated as shown in **Figure 8**. The magnetic field at 364 nm is concentrated at the interface between Ag and SiO_2. However, at 532 nm, it is concentrated at the interface between Ag and air. From these results, the propagating surface plasmon polariton is excited at the interface between Ag and the SiO_2 substrate at 364 nm and at the interface between Ag and the air substrate at 532 nm. Therefore, it is assumed that the peak transmission and the abrupt change of TM light are due to the exciting surface plasmon polariton at the two kinds of interfaces.

Finally, to confirm the change of the polarization states, the S-parameter for various structural periods on the Poincaré sphere was plotted. The Poincaré sphere with varying structural periods from 300 nm to 390 nm is shown in Figure 9. All plots are on the surface of the Poincaré sphere. It means these conditions are fully polarized. In an increasing structural period, the values of S_1 and S_3 are increasing. Between 345 and 350 nm, the sign of S_3 changes from negative to positive, meaning that the curve intersects the equator at this point, and the polarization state changes from elliptically polarized light to linearly polarized light. Therefore, it is believed that the arbitrary polarization state can be realized

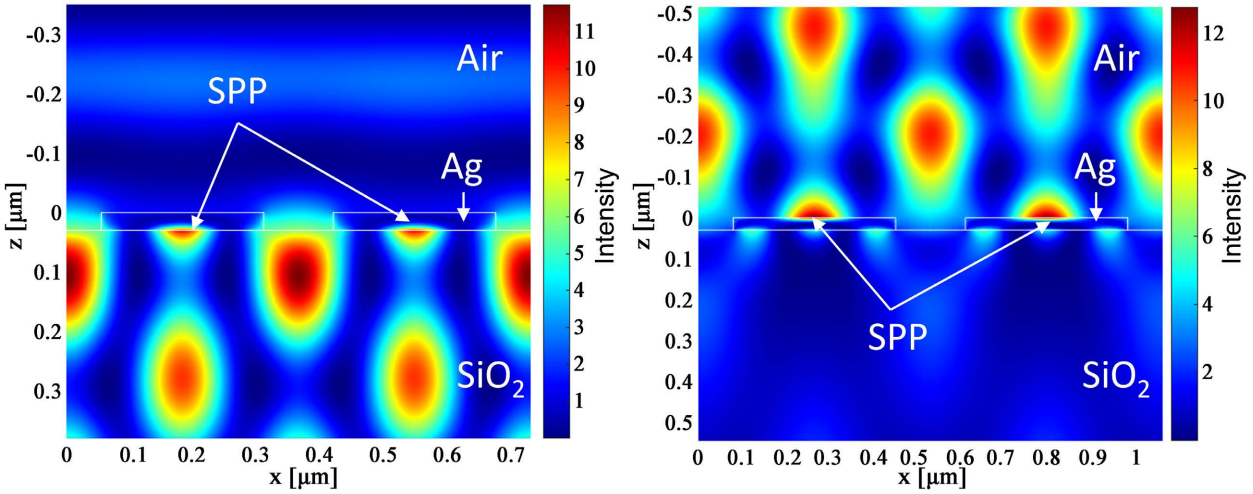

Figure 8. Intensity distribution of the magnetic field for (a) $P = 364$ nm and (b) $P = 532$ nm. For $P = 364$ nm, the magnetic field is concentrated at the interface between Ag and SiO_2. For $P = 532$ nm, the magnetic field is concentrated at the interface between Ag and air.

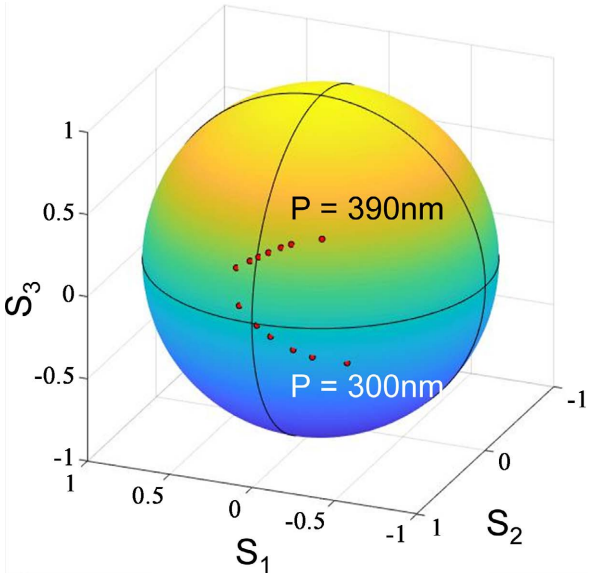

Figure 9. Poincaré sphere varying structural period from 300 nm to 390 nm. As structural period increases, the values of S_1 and S_3 increase. The polarization state changed from elliptically polarized light to linearly polarized light, because the sign of S_3 is changed from minus to plus between 345 and 350 nm.

by controlling the polarization state using the structure of the metal grating structure, which is a kind of plasmonic metasurface. We are currently conducting experiments to confirm the results of this simulation and plan to report those results in the future.

4. Conclusion

A polarization control device was developed using a plasmonic metasurface with the aim of achieving the desired polarization state. First, a simulation of the polarization control device was performed using the RCWA method, and it was shown that the transmittance and phase difference could be controlled by structural parameters such as the grating pitch and metal film thickness. Then, using the Senarmont method, the phase difference of the experimental devices consisting of a one-dimensional Ag diffraction grating fabricated by EBL and lift-off was determined. The results were almost the same as those obtained in the simulation. According to the transmittance mapping and the distribution of the magnetic field intensity, the peak transmittance and abrupt change of phase for TM light are caused by the excitation of the propagating surface plasmon resonance at one of two kinds of interfaces between Ag and SiO_2 or Ag and air. Finally, when the S-parameter was obtained from the simulation results and shown on the Poincaré sphere, it was shown that the arbitrary polarization state could be realized by controlling the polarization state using the device's structural parameters.

Acknowledgements

This work was supported by JSPS KAKENHI, Grant Number 20K05359 and Tateishi Science and Technology Foundation.

Conflicts of Interest

The authors declare no conflicts of interest regarding the publication of this paper.

References

[1] Hertz, H. (1893) Electric Waves. Macmillan and Company, Ltd., New York, 177.

[2] Bird, G.R. and Parrish Jr., M. (1960) The Wire Grid as a Near-Infrared Polarizer. *Journal of the Optical Society of America*, **50**, 886-891. https://doi.org/10.1364/JOSA.50.000886

[3] Hass, M. and O'Hara, M. (1965) Sheet Infrared Transmission Polarizers. *Applied Optics*, **4**, 1027-1031. https://doi.org/10.1364/AO.4.001027

[4] Auton, J.P. (1967) Infrared Transmission Polarizers by Photolithography. *Applied Optics*, **6**, 1023-1027. https://doi.org/10.1364/AO.6.001023

[5] Tamada, H., Doumuki, T., Yamaguchi, T. and Matsumoto, S. (1997) Al Wire-Grid Polarizer Using the *S*-Polarization Resonance Effect at the 0.8-μm-Wavelength Band. *Optics Letters*, **22**, 419-421. https://doi.org/10.1364/OL.22.000419

[6] Schlachter, F., Barnett, J., Plachetka, U., Nowak, C., Messerscmidt, M., Thesen, M.

and Kurz, H. (2016) UV-NIL Based Nanostructuring of Aluminum Using a Novel Organic Imprint Resist Demonstrated for 100 nm Half-Pitch Wire Grid Polarizer. *Microelectronic Engineering*, **155**, 118-121. https://doi.org/10.1016/j.mee.2016.03.046

[7] Yu, Z., Deshpande, P., Wu, W., Wang, J. and Chou, S.Y. (2000) Reflective Polarizer Based on a Stacked Double-Layer Subwavelength Metal Grating Structure Fabricated Using Nanoimprint Lithography. *Applied Physics Letters*, **77**, 927-929 https://doi.org/10.1063/1.1288674

[8] Yu, X.J. and Kwok, H.S. (2003) Optical Wire-Grid Polarizers at Oblique Angles of Incidence. *Journal of Applied Physics*, **93**, 4407-4412. https://doi.org/10.1063/1.1559937

[9] Xu, M.H., Urbach, P., de Boer, D.K.G. and Cornelissen, H.J. (2005) Wire-Grid Diffraction Gratings Used as Polarizing Beam Splitter for Visible Light and Applied in Liquid Crystal on Silicon. *Optics Express*, **13**, 2303-2305. https://doi.org/10.1364/OPEX.13.002303

[10] Qin, L., Yang, J., Wang, C., Shen, C., Wang, Y., Tang, J. and Liu, J. (2019) Preparation and Measurement of Subwavelength Bilayer Metal Wire Grid Polarizers on Flexible Plastic Substrates. *Optics Communications*, **434**, 118-123. https://doi.org/10.1016/j.optcom.2018.10.060

[11] Wang, J.J., Walters, F., Liu, X., Sciortino, P. and Deng, X. (2007) High-Performance, Large Area, Deep Ultraviolet to Infrared Polarizers Based on 40 nm Line/78 nm Space Nanowire Grids. *Applied Physics Letters*, **90**, Article No. 061104. https://doi.org/10.1063/1.2437731

[12] Ma, Y., Sun, N., Zhang, R., Guo, L., She, Y., Zheng, J. and Ye, Z. (2014) Integrated Color Filter and Polarizer Based on Two-Dimensional Superimposed Nanowire Arrays. *Journal of Applied Physics*, **116**, Article No. 044314. https://doi.org/10.1063/1.4891804

[13] Stenkamp, B., Abraham, M., Ehrfeld, W., Knapek, E., Hintemaier, M., Gale, M.T. and Morf, R. (2014) Nanofabrication Technologies and Device Integration. *Proceedings of SPIE—The International Society for Optical Engineering*, **2213**, 288-296.

[14] Ekinci, Y., Solak, H.H., David, C. and Sigg, H. (2006) Bilayer Al Wire-Grids as Broadband and High-Performance Polarizers. *Optics Express*, **14**, 2323-2334. https://doi.org/10.1364/OE.14.002323

[15] Ye, Z., Peng, Y., Zhai, T., Zhou, Y. and Liu, D. (2011) Surface Plasmon-Mediated Transmission in Double-Layer Metallic Grating Polarizers. *Journal of the Optical Society of America B*, **28**, 502-507. https://doi.org/10.1364/JOSAB.28.000502

[16] Ye, Z., Zheng, J., Sun, S., Chen, S. and Liu, D. (2013) Compact Color Filter and Polarizer of Bilayer Metallic Nanowire Grating Based on Surface Plasmon Resonances. *Plasmonics*, **8**, 555-559. https://doi.org/10.1007/s11468-012-9433-6

[17] Wang, J., Shen, Z. and Wu, W. (2017) Broadband and High-Efficiency Circular Polarizer Based on Planar-Helix Chiral Metamaterials. *Applied Physics Letters*, **111**, Article No. 113503. https://doi.org/10.1063/1.4990142

[18] Zhao, Y., Belkin, M.A. and Aliù, A. (2012) Twisted Optical Metamaterials for Planarized Ultrathin Broadband Circular Polarizers. *Nature Communications*, **3**, Article No. 870. https://doi.org/10.1038/ncomms1877

[19] Hsu, S.-Y., Lee, K.-L., Lin, E.-H., Lee, M.-C. and Wei, P.-K. (2009) Giant Birefringence Induced by Plasmonic Nanoslit Arrays. *Applied Physics Letters*, **95**, Article No. 013105. https://doi.org/10.1063/1.3167772

[20] Ishi, M., Iwami, K. and Umeda, N. (2015) An Au Nanofin Array for High Efficiency

Plasmonic Optical Retarders at Visible Wavelengths. *Applied Physics Letters*, **106**, Article No. 021115. https://doi.org/10.1063/1.4905369

[21] Ishi, M., Iwami, K. and Umeda, N. (2016) Highly-Efficient and Angle-Independent Zero-Order Half Waveplate at Broad Visible Wavelength Based on Au Nanofin Array Embedded in Dielectric. *Optics Express*, **24**, 7966-7976. https://doi.org/10.1364/OE.24.007966

[22] Djalalian-Assl, A., Cadusch, J.J., Teo, Z.Q., Davis, T.J. and Roberts, A. (2015) Surface Plasmon Wave Plates. *Applied Physics Letters*, **106**, Article No. 041104. https://doi.org/10.1063/1.4906596

[23] Motogaito, A., Nakajima, T., Miyake, H. and Hiramatsu, K. (2017) Excitation Mechanism of Surface Plasmon Polaritons in a Double-Layer Wire Grid Structure. *Applied Physics A*, **123**, Article No. 729. https://doi.org/10.1007/s00339-017-1367-6

[24] Motogaito, A., Morishita, Y., Miyake, H. and Hiramatsu, K. (2015) Extraordinary Optical Transmission Exhibited by Surface Plasmon Polaritons in a Double-Layer Wire Grid Polarizer. *Plasmonics*, **10**, 1657-1662. https://doi.org/10.1007/s11468-015-9980-8

[25] Motogaito, A., Mito, S., Miyake, H. and Hiramastsu, K. (2016) Detecting High-Refractive-Index Media Using Surface Plasmon Sensor with One-Dimensional Metal Diffraction Grating. *Optics and Photonics Journal*, **6**, 164-170. https://doi.org/10.4236/opj.2016.67018

[26] Motogaito, A. and Ito, Y. (2019) Excitation Mechanism of Surface Plasmon Polaritons for Surface Plasmon Sensor with 1D Metal Grating Structure for High Refractive Index Medium. *Photonic Sensors*, **9**, 11-18. https://doi.org/10.1007/s13320-018-0515-8

[27] Motogaito, A., Tanaka, R. and Hiramatsu, K. (2021) Fabrication of Perfect Plasmonic Absorbers for Blue and Near-Ultraviolet Lights Using Double-Layer Wire-Grid Structures. *Journal of the European Optical Society-Rapid Publications*, **17**, Article No. 6. https://doi.org/10.1186/s41476-021-00151-0

[28] Vansteenkiste, N., Vignolo, P. and Aspect, A. (1993) Optical Reversibility Theorems for Polarization: Application to Remote Control of Polarization. *Journal of the Optical Society of America A*, **10**, 2240-2245. https://doi.org/10.1364/JOSAA.10.002240

[29] Jullien, A., Albert, O., Chériaux, G., Etchepare, J., Kourtev, S., Minkovski, N. and Saltiel, S.M. (2005) Nonlinear Polarization Rotation of Elliptical Light in Cubic Crystals, with Application to Cross-Polarized Wave Generation. *Journal of the Optical Society of America B*, **22**, 2635-2641. https://doi.org/10.1364/JOSAB.22.002635

[30] Gao, C., Wang, B., Fu, C., Fang, J., Wen, K., Meng, Z., Nie, Z., Xing, X., Chen, L., Lei, L. and Zhou, J. (2020) Polarization-Controlled Grating Polarizer under Second Bragg Incidence with Silver Deposited in Groove. *Optics Communications*, **459**, Article No. 125063. https://doi.org/10.1016/j.optcom.2019.125063

[31] Wu, P.C., Zhu, W., Shen, Z.X., Chong, P.H.J., Ser, W., Tsai, D.P. and Liu, A.-Q. (2017) Broadband Wide-Angle Multifunctional Polarization Converter via Liquid-Metal-Based Metasurface. *Advanced Optical Materials*, **5**, Article No. 1600938. https://doi.org/10.1002/adom.201600938

[32] Mueller, J.P.B., Rubin, N.A., Devlin, R.C., Groever, B. and Capasso, F. (2017) Metasurface Polarization Optics: Independent Phase Control of Arbitrary Orthogonal States of Polarization. *Physical Review Letters*, **118**, Article No. 113901. https://doi.org/10.1103/PhysRevLett.118.113901

[33] Arbabi, A., Horie, Y., Bagheri, M. and Faraon, A. (2015) Dielectric Metasurfaces for Complete Control of Phase and Polarization with Subwavelength Spatial Resolution

and High Transmission. *Nature Nanotechnology*, **10**, 937-943. https://doi.org/10.1038/nnano.2015.186

[34] Lovera, P., Jones, D., Corbett, B. and O'Riordan, A. (2012) Polarization Tunable Transmission through Plasmonic Arrays of Elliptical Nanopores. *Optics Express*, **20**, 25325-25332. https://doi.org/10.1364/OE.20.025325

[35] Yan, T., Ma, Q. and Cui, T. (2020) Circular Polarization Hologram Realized by Pancharatnam-Berry Phase in Microwave Frequency. *Journal of Computer and Communications*, **8**, 134-141. https://doi.org/10.4236/jcc.2020.812013

[36] Juhl, M., Mendoza, C., Mueller, J.P.B., Capasso, F. and Leosson, K. (2017) Performance Characteristics of 4-Port In-Plane and Out-of-Plane In-Line Metasurface Polarimeters. *Optics Express*, **25**, 28697-28709. https://doi.org/10.1364/OE.25.028697

[37] Mueller, J.P., Lesson, B.K. and Capasso, F. (2016) Ultracompact Metasurface In-Line Polarimeter. *Optica*, **3**, 42-47. https://doi.org/10.1364/OPTICA.3.000042

[38] Jiao, S., Yu, W., Stoica, G. and Wang, L.V. (2003) Contrast Mechanisms in Polarization-Sensitive Mueller-Matrix Optical Coherence Tomography and Application in Burn Imaging. *Applied Optics*, **42**, 5191-5197. https://doi.org/10.1364/AO.42.005191

[39] Giattina, S.D., Courtney, B.K., Herz, P.R., Harman, M., Shortkroff, S., Stamper, D.L., Liu, B., Fujimoto, J.G. and Berzinski, M.E. (2006) Assessment of Coronary Plaque Collagen with Polarization Sensitive Optical Coherence Tomography (PS-OCT). *International Journal of Cardiology*, **107**, 400-409. https://doi.org/10.1016/j.ijcard.2005.11.036

[40] Torres, R., Kaempfe, T., Delaigue, M., Parriaux, O., Hönninger, C., Lopez, J., Kling, R. and Mottay, E. (2013) Influence of Laser Beam Polarization on Laser Micro-Machining of Molybdenum. *Journal of Laser Micro/Nanoengineering*, **8**, 188-191. https://doi.org/10.2961/jlmn.2013.03.0001

[41] Ye, Y., Zhou, Y., Zhang, H. and Chen, L. (2011) Polarizing Color Filter Based on a Subwavelength Metal-Dielectric Grating. *Applied Optics*, **50**, 1356-1363. https://doi.org/10.1364/AO.50.001356

[42] Amaya, J.S., González, C. and Bailon, K. (2021) Web Control System for Transcorneal Electric Stimulation Devices. *Journal of Biomedical Science and Engineering*, **14**, 452-459. https://doi.org/10.4236/jbise.2021.1412039